Photoluminescence and Raman mapping of β‑Ga$_2$O$_3$

Cassandra Remple, Jesse Huso and Matthew D. McCluskey

View Online   Export Citation   CrossMark

AIP Advances

Call For Papers!

SPECIAL TOPIC: Advances in Low Dimensional and 2D Materials

Photoluminescence and Raman mapping of β-Ga₂O₃

View Online   Export Citation   CrossMark

Cassandra Remple,[1,2] (iD) Jesse Huso,[3] (iD) and Matthew D. McCluskey[1,2,3,a)] (iD)

AFFILIATIONS

[1] Department of Physics and Astronomy, Washington State University, Pullman, Washington 99164-2814, USA
[2] Materials Science and Engineering Program, Washington State University, Pullman, Washington 99164-2711, USA
[3] Klar Scientific, 1615 Northeast Eastgate Blvd., Unit G, Ste. 3E, Pullman, Washington 99163-5300, USA

[a)] Author to whom correspondence should be addressed: mattmcc@wsu.edu

ABSTRACT

The semi-insulating single crystal β-Ga₂O₃ is becoming increasingly useful as a substrate for device fabrication. Fe doping is a method for producing such substrates. Along with Fe dopants, β-Ga₂O₃:Fe also contains Cr^{3+}. Photoluminescence (PL) emission peaks at 690 nm (1.80 eV) and 696 nm (1.78 eV), as well as a broad feature around 709 nm (1.75 eV), are observed in β-Ga₂O₃:Fe. PL mapping of the 690 nm emission showed high and low intensity bands due to impurity striations introduced during crystal growth. PL mapping also revealed surface defects showing broad emissions around 983 nm (1.26 eV) and 886 nm (1.40 eV) that were spatially localized, occurring at discrete spots on the sample surface. Raman mapping of an 886 nm emission center revealed peaks at 2878 and 2930 cm^{-1}, consistent with an organometallic or hydrocarbon compound. Raman mapping of the 983 nm center showed a peak at 2892 cm^{-1}. Bright UV emission centers showed Raman peaks at 2910 and 2968 cm^{-1}, which are attributed to Si–CH₃ groups that may originate from silica polishing compounds or annealing in a silica ampoule.

I. INTRODUCTION

Monoclinic gallium oxide (β-Ga₂O₃) exhibits an optical bandgap of 4.8 or 4.5 eV for light polarized along the b or c axis, respectively.[1,2] This ultrawide bandgap makes it a good material for power electronics, which requires a high breakdown field.[1,3] Ga₂O₃ can be made n-type conducting with extrinsic doping of Sn, Si, Zr, Hf, and Ge, enabling field effect transistor (FET) devices.[3,4] Ga₂O₃ has also been made semi-insulating using Fe, Mg, N, and Zn dopants, which behave as deep acceptors.[1,3,5–8] In this study, the focus is on Fe^{3+} dopants (3d^5) and Cr^{3+} impurities (3d^3), although Fe can also be an unintentional impurity.[9,10] Fe-doped β-Ga₂O₃ crystals are of interest as substrates and buffer layers in high-power FETs. They have shown significantly higher electrical breakdown fields than GaN-based or SiC-based FETs.[9,11–14] Fe can occupy two sites, the Ga(I) and Ga(II) sites. The Ga(II), or octahedral, site is considered to be more energetically favorable.[1,15]

Cr^{3+} in β-Ga₂O₃ has defect absorption bands at 430 nm (2.88 eV) and 600 nm (2.07 eV), which is similar to the absorption of ruby (Al₂O₃:Cr^{3+}).[16–19] The two absorption bands at 430 and 600 nm correspond to $^4A_2 \rightarrow {}^4T_1$ and $^4A_2 \rightarrow {}^4T_2$ transitions,

respectively.[16,17,20,21] Cr^{3+} in Ga₂O₃ also has emission spectra similar to those of ruby, which has R_1 and R_2 lines at 694 and 693 nm (1.787 and 1.789 eV), respectively.[16,22,23] The β-Ga₂O₃ Cr^{3+} emission spectrum consists of a broad red peak around 710 nm with two sharp peaks at 688 and 696 nm, ascribed to the $^2E \rightarrow {}^4A_2$ and $^4T_2 \rightarrow {}^4A_2$ internal Cr^{3+} transitions for the sharp and broad peaks, respectively.[16–18,20,24,25]

In α-Ga₂O₃, isomorphous with α-Al₂O₃ (corundum), there is a competition between the luminescence of Cr^{3+} and Fe^{3+}, with the Fe^{3+} emission observed at 950 nm (1.305 eV).[26] Similarly, Sun et al.[17] suggested that there is an energy transfer process in which electron–hole pairs in β-Ga₂O₃ recombine by transferring energy to Cr^{3+} and also Fe^{3+}, which then returns to its ground state by exciting Cr^{3+}.[27]

II. EXPERIMENTAL

An Fe-doped (100) β-Ga₂O₃ crystal grown by the Czochralski (CZ) method was obtained from Synoptics, Inc. The crystal was grown along the [010] direction, perpendicular to the (100) and (001) cleavage planes.[28] For the present study, the sample was

cleaved along the (100) plane from the boule. The sample underwent a chemical mechanical polish (CMP) with colloidal silica. Prior work on the same sample showed Cr^{3+} emission lines.[17] Photoluminescence (PL) and photoluminescence excitation (PLE) spectra were measured using a Horiba Jobin-Yvon FluoroLog-3 spectrometer with double-grating monochromators and a photomultiplier tube. The excitation source is a broadband 450 W xenon continuous-wave gas discharge lamp. Excitation wavelengths of 240–600 nm were selected by passing light through a monochromator. Measurements were performed at room temperature. While PL spectra show emission for a specific excitation, the PLE measurement collects light emitted at a specified wavelength and plots the intensity of this emission vs excitation wavelength. These PL and PLE measurements were not spatially resolved and therefore give an average PL spectrum.

PL mapping was carried out on the (100) face using a Klar Mini Pro microscope with 355 nm laser excitation. A spectrometer was selected to cover the spectral region of interest. Previous results showed that 355 nm photons excite a strong 3.27 eV emission in Ga_2O_3.[29] While the 3.27 eV emission was outside the spectrometer range, the emission was detectable through a second-order grating reflection and corresponds with previous results, showing a highly localized distribution. Spectra were collected using a spatial step size of 2 μm. Spectral fitting was performed using Graphics Processing Unit (GPU) accelerated fitting. A custom model consisting of Gaussian and bi-Gaussian functions was used to match the observed spectral features of the sample (supplementary material, Figs. S.1 and S.2). Maps of the fitted spectral parameters were then plotted as a false-color image.

Raman mapping was carried out in correlation with the PL mapping such that the discrete emission regions could be correlated with specific Raman peaks. This was carried out using a Klar Mini Pro microscope with a 532 nm laser excitation. Spectra were

collected using a spatial step size of 2 μm (same as the PL map). A custom model consisting of Voigt functions and a bi-Gaussian background was used to match the observed spectral features of the sample (supplementary material, Fig. S.3). For the bright emitter investigation, we performed Raman mapping on a sample previously studied by Huso *et al.*[29] This sample was an unintentionally doped (UID) β-Ga_2O_3 bulk single crystal, grown at Tamura Inc., Japan, by the edge-defined film-fed growth (EFG) method. The sample measured had been annealed in a hydrogen atmosphere in a closed ampoule at 950 °C.[29]

III. RESULTS AND DISCUSSION

A. PL and PLE of Cr^{3+}

The emission spectrum [Fig. 1(a)] showed sharp peaks due to Cr^{3+} defects in Ga_2O_3 at 690 nm (1.80 eV) and 696 nm (1.78 eV) and a broad emission feature at 709 nm (1.75 eV). These peaks are consistent with a previous work.[17] The PLE spectrum at 715 nm [Fig. 1(b)] shows strong defect absorption bands at 430 nm (2.9 eV) and 600 nm (2.0 eV). These both agree with Cr^{3+} absorption in Ga_2O_3 reported by Tippins.[16] There is also a band edge onset around 280 nm (4.43 eV), which is close to the reported band-to-band transition.[16]

B. Spatially resolved PL imaging of Cr^{3+}

Spatially resolved PL was performed to observe the defect emission across the sample. The Cr^{3+} peak intensity within the PL map shows an extremely tight correlation with the intensity of the broad Cr^{3+} emission (Fig. 2 and supplementary material, Fig. S.1). Cr^{3+} striations, which appear as diagonal stripes in Fig. 2, are seen as variations in the PL emission intensity. These striations formed at an angle to the growth direction, which was along the *b* axis (Fig. 2).
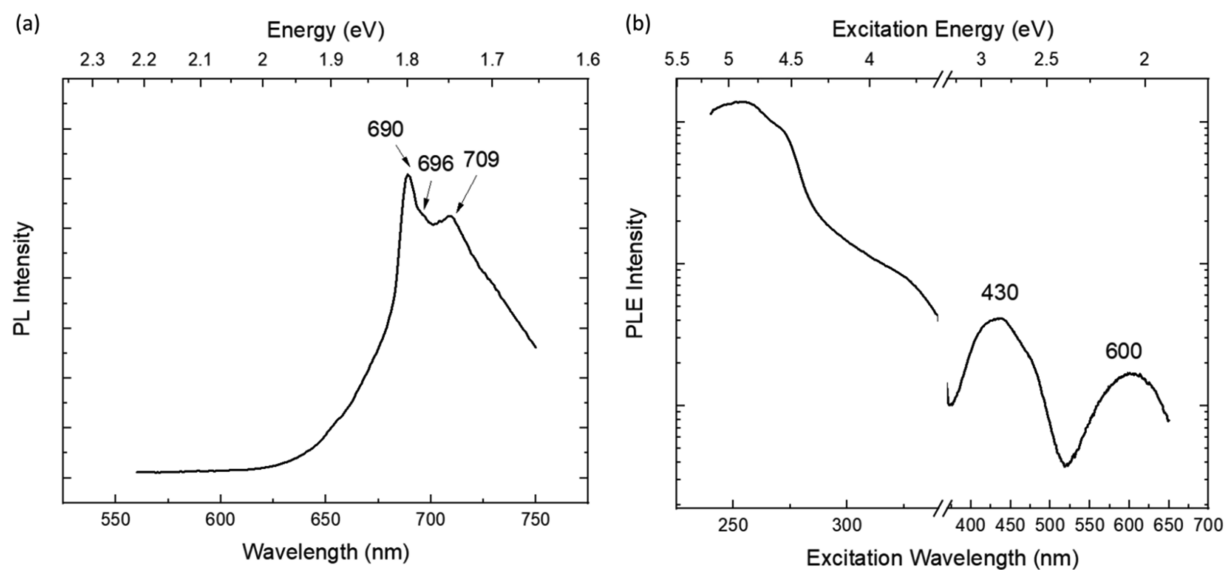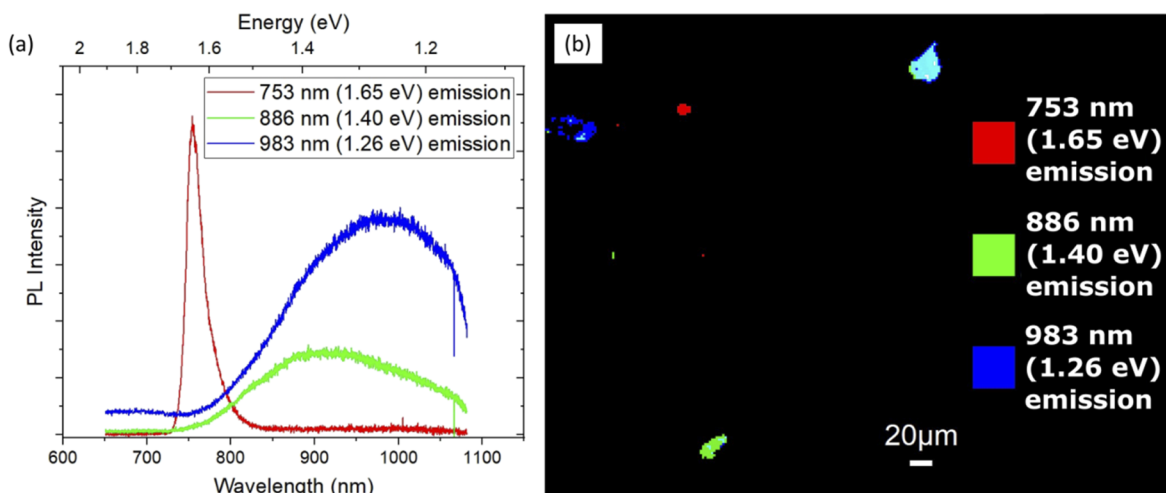

FIG. 1. (a) PL spectrum of Fe-doped β-Ga_2O_3 crystal under excitation of 260 nm. (b) PLE spectrum of Fe-doped β-Ga_2O_3 crystal for PL at 715 nm. Line breaks on horizontal axes are to avoid second-order reflection of the excitation wavelength.
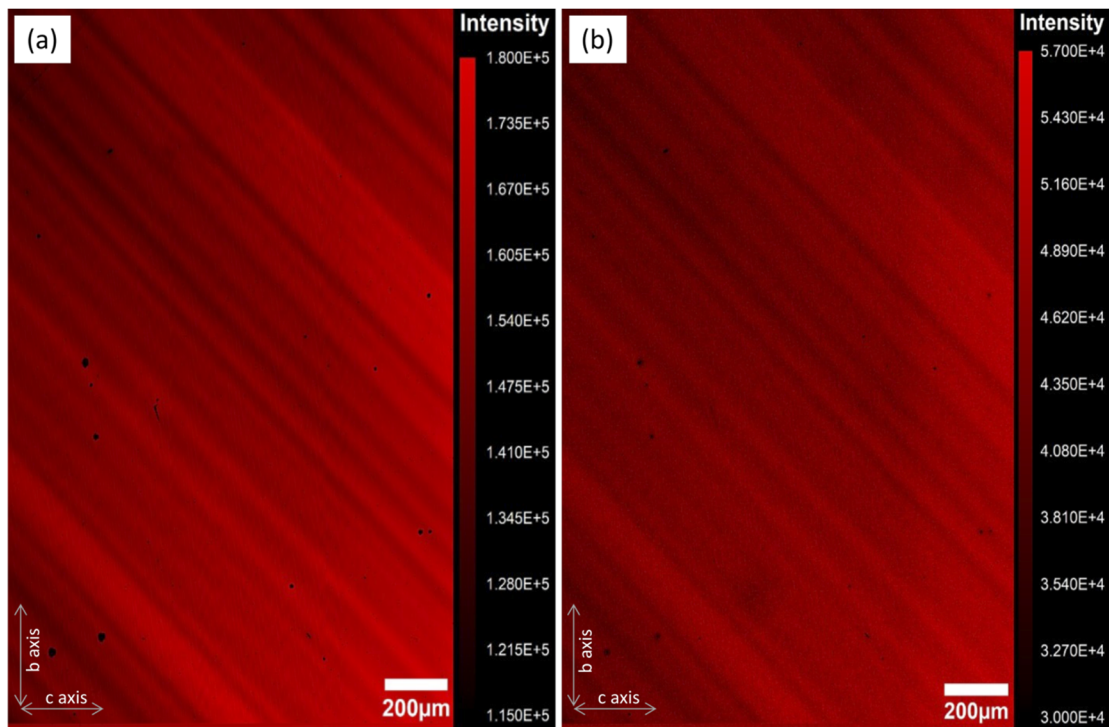
FIG. 2. Map of the PL intensity of the (a) broad and (b) sharp Cr^{3+} emission at 355 nm excitation. Black spots are regions where there were brighter emissions at different wavelengths that obscured the Cr^{3+} spectra.

Impurity striations, or variations in the concentration of a net impurity across the axis of a crystal, are considered to be an undesirable effect of crystals grown from a melt.[30] One possible mechanism involves imperfect crystal rotatio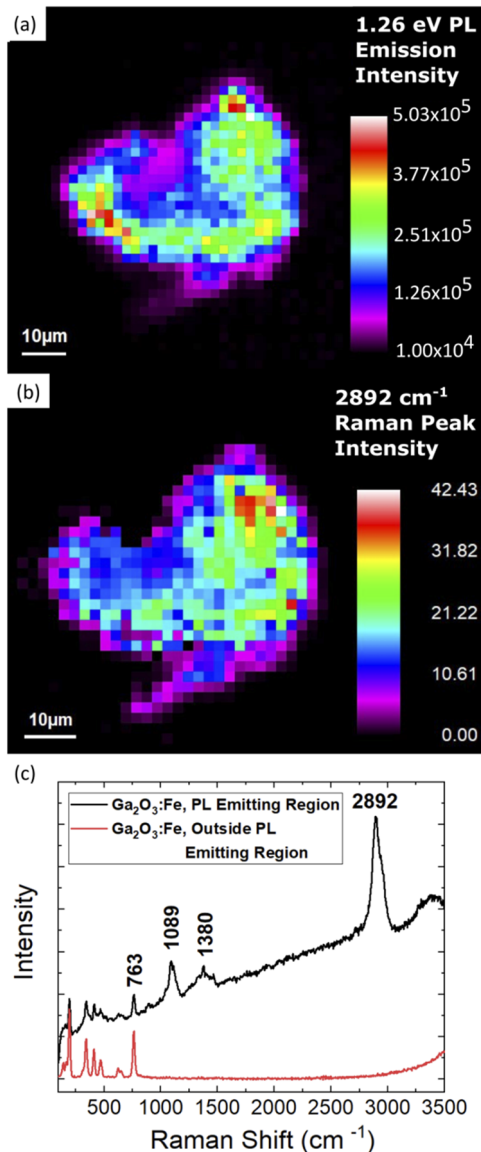n where the solid/liquid interface of the melt passes through colder and hotter spots. If the melt is not homogeneous in temperature, it can lead to some level of dopant segregation, which will appear periodic according to the rotation of the crystal.

FIG. 3. (a) PL spectra of Fe-doped β-Ga_2O_3 crystal under excitation of 355 nm resulting from the PL mapping. The 1.65 eV emission is a second-order grating reflection from the 3.27 eV emission. (b) Three-color map of the different emitting regions observed under 355 nm excitation. Note that the upper right center is a combination of the 1.40 and 1.26 eV emissions, which is why it is teal, a combination of green and blue.

C. Spatially resolved PL showing localized emissions

PL mapping showed three different localized emissions randomly distributed across the sample, with no apparent relationship to the Cr^{3+} emission. The emissions mostly occurred in isolated cases, where only a single emission peak was observed. Occasionally, there were overlapping emitting regions where all three emissions appeared in clusters. Curve fitting indicated that the centroids are 1.646, 1.399, and 1.262 eV (753, 886, and 983 nm). We refer to these emissions as 1.65, 1.40, and 1.26 eV.

The bright, localized near-UV emission [3.27 eV (379 nm)] was observed on the surface of Ga_2O_3 when excited by photons with energies above 3.4 eV (365 nm).[29] We refer to these as "bright emitters." Due to second-order grating reflection, these bright emitters appear as a 1.65 eV emission. Consistent with prior work,[29] the emitting regions are not distributed homogenously through Ga_2O_3 but instead at localized spots (Fig. 3).

FIG. 4. (a) PL map of the 1.26 eV emitting region at 355 nm excitation. (b) Raman map of the 2892 cm^{-1} peak intensity at 532 nm excitation for the same emitting region in (a). (c) Raman spectra examples for spots inside the 1.26 eV PL emitting region and outside the emitting region.
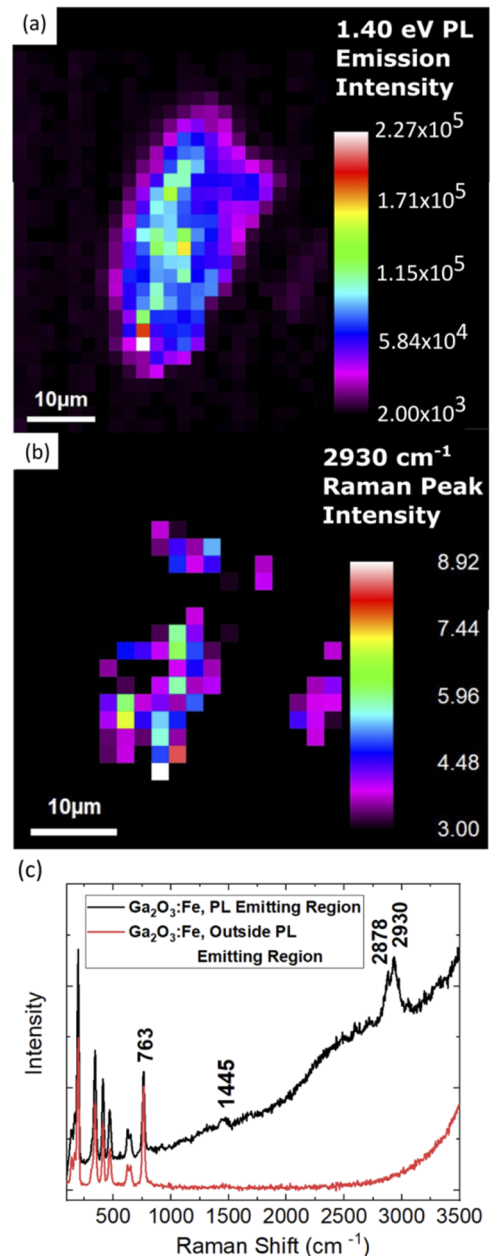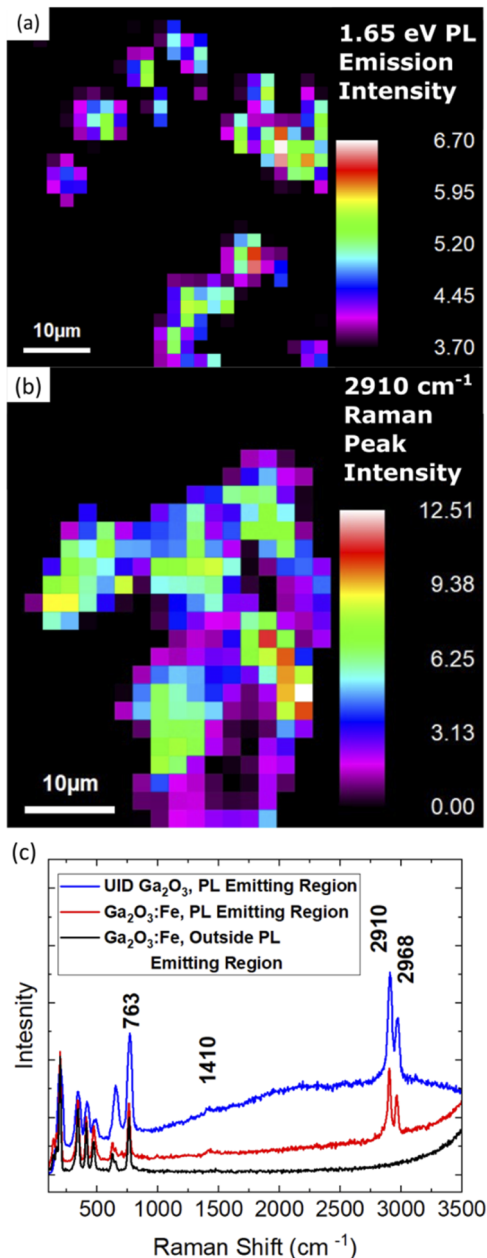

FIG. 5. (a) PL map of the 1.40 eV emitting region at 355 nm excitation. (b) Raman map of the 2930 cm^{-1} peak intensity at 532 nm excitation for the same emitting region in (a). (c) Raman spectra examples for spots inside 1.40 eV PL emitting region and outside the emitting region.

1. Raman mapping

Raman mapping was performed to help determine the chemical composition of the different emitting regions. An example of the 1.26 eV (983 nm) emitting region is shown in Fig. 4(a). Figures 4(a)

FIG. 6. (a) PL map of the 1.65 eV emitting region at 355 nm excitation on β-Ga$_2$O$_3$:Fe grown by Synoptics. The 1.65 eV peak is a second-order grating reflection of the 3.27 eV "bright emitter." (b) Raman map of the 2910 cm^{-1} peak at 532 nm excitation for the same emitting region as in (a). (c) Raman spectra of the 1.65 eV PL emitting regions for β-Ga$_2$O$_3$:Fe grown by Synoptics and a UID sample grown by Tamura. A spectrum is also shown for the β-Ga$_2$O$_3$:Fe sample at a spot outside the 1.65 eV emitting region.

and 4(b) show excellent agreement of feature shape and size, indicating that the PL and Raman signatures arise from the same defect. The maps also correlate with microscope images of the emission centers (supplementary material, Figs. S.4–S.6). The Raman spectra associated with the higher intensity points of these maps showed typical β-Ga$_2$O$_3$ Raman spectral features between 100 to 1000 cm^{-1}.[31] The peak at 763 cm^{-1} is distinctive and was typically a strong Ga$_2$O$_3$ peak. However, an additional peak is observed at 2892 cm^{-1} as well as two smaller features at 1089 and 1380 cm^{-1}. These peaks are likely related to a hydrocarbon compound although a specific identification has not been made.[32]

Similarly, the 1.40 eV emission center [Figs. 5(a) and 5(b)] shows a correlation between the PL and Raman maps. This emitting region had two strong peaks at 2930 and 3060 cm^{-1}, as well as a smaller peak at 1445 cm^{-1}. Occasionally, there was a peak at 1600 cm^{-1}, which indicates carbon,[33–35] and the other peaks are likely associated with hydrocarbons.[32]

An example of the 1.65 eV center (second-order peak of the 3.27 eV emission) can be seen in Fig. 6(a). This emission was originally observed by Huso et al.,[29] who studied an unintentionally doped (UID) β-Ga$_2$O$_3$ sample that had been annealed in hydrogen at 950 °C. The emissions increased in concentration on the sample surface with this hydrogen anneal.[29] In the present work, the Fe-doped sample was not hydrogen annealed and therefore has a low concentration of the 1.65 eV emitting regions. However, the emitting regions in both samples show the same PL and Raman spectra [Fig. 6(c)]. There are two strong peaks at 2910 and 2968 cm^{-1}, as well as a smaller peak at 1410 cm^{-1}.

A close spectral match can be seen with that of the siloxane polymer, or silicone grease.[36] The peaks have been identified as Si–CH$_3$ bond deformation (1410 cm^{-1}) and Si–CH$_3$ stretching in and out of phase (2910 and 2968 cm^{-1}). However, there was no apparent source of silicone grease for these samples. The Ga$_2$O$_3$:Fe sample underwent a chemical mechanical polish (CMP) with colloidal silica, which could lead to these Raman modes. CMP often has propylene or ethylene glycol as a passivation agent, and therefore, the Si–CH$_3$ bond could result from that. The UID Ga$_2$O$_3$ sample did not undergo polishing but was hydrogen annealed in a silica ampoule, which may have been the source for Si surface contamination.[37] Energy dispersive spectroscopy showed evidence for Si on the surface of the sample (see the supplementary material in Ref. 29), consistent with the Raman results. Given that two samples with different histories (CMP vs hydrogen anneal) showed these characteristic Raman peaks, the formation of Si–CH$_3$ may be a common, energetically favorable occurrence. Additional work is needed to determine the formation mechanism for this Si–CH$_3$ compound.

IV. CONCLUSIONS

In conclusion, PL and Raman mapping of a β-Ga$_2$O$_3$:Fe sample showed that emissions are not spatially uniform across the surface of the sample. This inhomogeneity includes Cr^{3+} impurity striations, which are observed as variations in the PL emission intensity. PL mapping also revealed surface defects showing broad emissions around 983 nm (1.26 eV) and 886 nm (1.40 eV) that were both highly localized, occurring at discrete spots on the sample surface. It is also apparent that these emissions have no relationship to the Cr^{3+} emissions observed. Raman mapping of an 886 nm

emission center revealed peaks at 2930 and 3060 cm^{-1}, consistent with an organometallic or hydrocarbon compound. Raman mapping of the 983 nm center showed a peak at 2892 cm^{-1}, likely related to hydrocarbon compounds. Finally, the bright emission center at 379 nm (3.27 eV) was observed as a second-order grating reflection peak at 753 nm (1.65 eV). These "bright emitters" showed Raman peaks at 2910 and 2968 cm^{-1}, which are signatures of Si–CH$_3$. The emitters may be created by surface polishing with colloidal silica or other Si-related contamination.

SUPPLEMENTARY MATERIAL

See the supplementary material for additional PL maps, widefield microscope images of the emission centers, and details on spectral fitting.

ACKNOWLEDGMENTS

AUTHOR DECLARATIONS

Conflict of Interest

J.H. is an employee of Klar Scientific, and MDM owns equity in the company.

DATA AVAILABILITY

The data that support the findings of this study are available from the corresponding author upon reasonable request.

REFERENCES

[1] M. D. McCluskey, J. Appl. Phys. 127, 101101 (2020).
[2] H. Peelaers and C. G. Van de Walle, Phys. Status Solidi B 252, 828 (2015).
[3] M. Higashiwaki, K. Sasaki, A. Kuramata, T. Masui, and S. Yamakoshi, Appl. Phys. Lett. 100, 013504 (2012).
[4] K. D. Chabak, K. D. Leedy, A. J. Green, S. Mou, A. T. Neal, T. Asel, E. R. Heller, N. S. Hendricks, K. Liddy, A. Crespo, N. C. Miller, M. T. Lindquist, N. A. Moser, R. C. Fitch, D. E. Walker, D. L. Dorsey, and G. H. Jessen, Semicond. Sci. Technol. 35, 013002 (2020).
[5] M. H. Wong, C.-H. Lin, A. Kuramata, S. Yamakoshi, H. Murakami, Y. Kumagai, and M. Higashiwaki, Appl. Phys. Lett. 113, 102103 (2018).
[6] J. R. Ritter, J. Huso, P. T. Dickens, J. B. Varley, K. G. Lynn, and M. D. McCluskey, Appl. Phys. Lett. 113, 052101 (2018).
[7] Y. K. Frodason, K. M. Johansen, L. Vines, and J. B. Varley, J. Appl. Phys. 127, 075701 (2020).
[8] T. D. Gustafson, J. Jesenovec, C. A. Lenyk, N. C. Giles, J. S. McCloy, M. D. McCluskey, and L. E. Halliburton, J. Appl. Phys. 129, 155701 (2021).
[9] S. J. Pearton, J. Yang, P. H. Cary, F. Ren, J. Kim, M. J. Tadjer, and M. A. Mastro, Appl. Phys. Rev. 5, 011301 (2018).
[10] B. E. Kananen, L. E. Halliburton, K. T. Stevens, G. K. Foundos, and N. C. Giles, Appl. Phys. Lett. 110, 202104 (2017).
[11] M. A. Mastro, A. Kuramata, J. Calkins, J. Kim, F. Ren, and S. J. Pearton, ECS J. Solid State Sci. Technol. 6, P356 (2017).
[12] S. J. Pearton, F. Ren, M. Tadjer, and J. Kim, J. Appl. Phys. 124, 220901 (2018).
[13] A. Y. Polyakov, N. B. Smirnov, I. V. Shchemerov, S. J. Pearton, F. Ren, A. V. Chernykh, and A. I. Kochkova, Appl. Phys. Lett. 113, 142102 (2018).
[14] A. Y. Polyakov, N. B. Smirnov, I. V. Schemerov, A. V. Chernykh, E. B. Yakimov, A. I. Kochkova, A. N. Tereshchenko, and S. J. Pearton, ECS J. Solid State Sci. Technol. 8, Q3091 (2019).
[15] M. E. Ingebrigtsen, J. B. Varley, A. Yu. Kuznetsov, B. G. Svensson, G. Alfieri, A. Mihaila, U. Badstübner, and L. Vines, Appl. Phys. Lett. 112, 042104 (2018).
[16] H. H. Tippins, Phys. Rev. 137, A865 (1965).
[17] R. Sun, Y. K. Ooi, P. T. Dickens, K. G. Lynn, and M. A. Scarpulla, Appl. Phys. Lett. 117, 052101 (2020).
[18] Y. F. Lv, J. Y. Xiang, F. S. Wen, W. M. Lv, W. T. Hu, and Z. Y. Liu, J. Magn. Magn. Mater. 377, 460 (2015).
[19] H. C. Seat and J. H. Sharp, IEEE Trans. Instrum. Meas. 53, 140 (2004).
[20] V. Vasyltsiv, A. Luchechko, L. Zhydachevskyy, R. Kostyk, R. Lys, D. Slobodzyan, R. Jakieła, B. Pavlyk, and A. Suchocki, J. Vac. Sci. Technol. A 39, 033201 (2021).
[21] Y. Tokida and S. Adachi, J. Appl. Phys. 112, 063522 (2012).
[22] A. L. Schawlow, J. Appl. Phys. 33, 395 (1962).
[23] W. Luhs and B. Wellegehausen, OSA Continuum 2, 184 (2019).
[24] I. Hany, G. Yang, C. E. Zhou, C. Sun, K. Gundogdu, D. Seyitliyev, E. O. Danilov, F. N. Castellano, D. Sun, and E. Vetter, Mater. Lett. 257, 126744 (2019).
[25] J. E. Stehr, M. Jansson, D. M. Hofmann, J. Kim, S. J. Pearton, W. M. Chen, and I. A. Buyanova, Appl. Phys. Lett. 119, 052101 (2021).
[26] G. T. Pott and B. D. McNicol, J. Lumin. 6, 225 (1973).
[27] J. J. Krebs and W. G. Maisch, Phys. Rev. B 4, 757 (1971).
[28] J. D. Blevins, K. Stevens, A. Lindsey, G. Foundos, and L. Sande, IEEE Trans. Semicond. Manuf. 32, 466 (2019).
[29] J. Huso, M. D. McCluskey, Y. Yu, M. M. Islam, and F. Selim, Sci. Rep. 10, 21022 (2020).
[30] M. D. McCluskey and E. E. Haller, Dopants and Defects in Semiconductors, 2nd ed. (CRC Press; Taylor & Francis Group, Boca Raton, FL, 2018).
[31] T. Onuma, S. Fujioka, T. Yamaguchi, Y. Itoh, M. Higashiwaki, K. Sasaki, T. Masui, and T. Honda, J. Cryst. Growth 401, 330 (2014).
[32] P. Larkin, Infrared and Raman Spectroscopy (Elsevier, 2011), pp. 1–5.
[33] M. Vázquez Piñón, B. Cárdenas Benítez, B. Pramanick, V. H. Perez-Gonzalez, M. J. Madou, S. O. Martinez-Chapa, and H. Hwang, Sens. Actuators, A 262, 10 (2017).
[34] L. T. Duy, D.-J. Kim, T. Q. Trung, V. Q. Dang, B.-Y. Kim, H. K. Moon, and N.-E. Lee, Adv. Funct. Mater. 25, 883 (2015).
[35] T. Takami, S. Ogawa, H. Sumi, T. Kaga, A. Saikubo, E. Ikenaga, M. Sato, M. Nihei, and Y. Takakuwa, e-J. Surf. Sci. Nanotechnol. 7, 882 (2009).
[36] P. Larkin, Infrared and Raman Spectroscopy (Elsevier, 2011).
[37] Z. Feng, A. F. M. A. U. Bhuiyan, Z. Xia, W. Moore, Z. Chen, J. F. McGlone, D. R. Daughton, A. R. Arehart, S. A. Ringel, S. Rajan, and H. Zhao, Phys. Status Solidi RRL 14, 2000145 (2020).